



# First Detailed Analysis of a Relatively Deep, Low Mass-ratio Contact Binary: ATO J108.6991+27.8306

Shuo Ma<sup>1,2,3</sup> , Jinzhong Liu<sup>1,2</sup>, Yu Zhang<sup>1,2</sup>, Guoliang Lü<sup>4</sup>, Ting Wu<sup>1,2</sup>, and Chenyang He<sup>4</sup>

<sup>1</sup>Xinjiang Astronomical Observatory, Chinese Academy of Sciences, Urumqi 830011, China; [liujinzh@xao.ac.cn](mailto:liujinzh@xao.ac.cn)

<sup>2</sup>University of Chinese Academy of Sciences, Beijing 100049, China

<sup>3</sup>Department of Astronomy, Xiamen University, Xiamen 361005, China

<sup>4</sup>School of Physical Science and Technology, Xinjiang University, Urumqi 830064, China

Received 2022 August 5; revised 2022 December 19; accepted 2023 January 6; published 2023 February 28

## Abstract

We present the first detailed photometric analysis of ATO J108.6991+27.8306 (hereinafter as J108). The short-period close binary J108 was observed by the Nanshan 1 m Wide Field Telescope of the Xinjiang Astronomical Observatory. The obtained *BVRI*-band light curves were used to determine the photometric solution by using the 2003 version of the Wilson-Devinney code. J108 is a typical deep ( $f > 50\%$ ), low mass ratio ( $q < 0.25$ ) overcontact binary system with a mass ratio of  $q = 0.1501$  and a fill-out factor of  $f = 50.1\%$ , suggesting that it is in the late evolutionary stage of contact binary systems. We found the target to be a W-type W UMa binary and provided evidence for the presence of starspots on both components. From the temperature-luminosity diagram, the main component is the evolved main sequence star with an evolutionary age of about 7.94 Gyr.

*Key words:* (stars:) binaries (including multiple): close – (stars:) binaries: eclipsing – stars: evolution – stars: individual (ATO J108.6991+27.8306)

## 1. Introduction

W Urase Majoris-type (W UMa) binaries are usually contact binary systems in which both components fill the Roche lobe during their main sequence evolutionary phase and share a common envelope (Lucy 1968; Stepien 2006), so that both components have approximate surface temperatures. W UMa binaries, whose component spectral types typically range from F to K, may have magnetic activity, such as starspots (Panchal & Joshi 2021; Poro et al. 2021; Ma et al. 2022). In addition, W UMa binaries with more massive components but at lower temperatures are defined as W-type W UMa binaries, and the opposite as A-type (Binnendijk 1970). The orbital period of the W UMa system is usually variable. The mass transfer between the two components (Hoffman et al. 2006; Meng et al. 2021) can cause the orbital period to increase or decrease. The magnetic braking effect (Lanza et al. 1998; Belloni et al. 2020) causes a loss of orbital angular momentum, which is expressed as a decrease in the orbital period. The magnetic cycle (Borkovits et al. 2005; Khaliullina 2018) and the third body (Shi et al. 2020) are responsible for the cyclic variation of the orbital period.

There are deep ( $f > 50\%$ ), low mass ratio ( $q < 0.25$ ) (DLMR) overcontact binaries (Qian et al. 2006; Yang & Qian 2015) among W Urase Majoris-type binaries, which are at the evolutionary stage of late short-period close binaries. These binaries are important for the study of stellar astrophysics because they may be the progenitors of single rapidly rotating

stars (Jiang 2020), such as Blue Straggler (BS) stars (Perets & Fabrycky 2009; Wei et al. 2021) and FK Com-type stars (Bopp & Stencel 1981; Sikora et al. 2020).

ATO J108.6991+27.8306 (TIC 155 709 042, LPSEB3, UCAC4 590-039991, ASASSN-V J071447.79+274950.6) (hereinafter as J108) was defined as close binary with an orbital period of 0.393 204 days by Heinze et al. (2018). Furthermore, J108 was first identified as an EW type binaries by All-Sky Automated Survey for Supernovae (ASAS-SN, Jayasinghe et al. 2019) and confirmed by Chen et al. (2020). At the same time, this target was included in the LAMOST catalog (Yang et al. 2020) and no more studies have been carried out on J108 since then. In this paper, we found that J108 is a member of the DLMR and attempted to perform the first public analysis of this interesting and unusual target.

## 2. Observations and Data Reduction

J108 was observed on 2020 December 23 using the Nanshan One-meter Wide-field Telescope (Bai et al. 2020, hereinafter as NOWT) of the Xinjiang Astronomical Observatory. During our observations, a standard Johnson-Cousins *BVRI* filter was used. Individual observations included 107 in the *B* filter, 107 in *V*, 105 in *R*, 112 in *I* and a total of 426 CCD images were acquired. These CCD images correspond to exposure times of 70, 40, 45, 50 s for the four bands of *BVRI*, respectively, with the observational accuracy better than 0.006 mag.

**Table 1**  
Observing Details of the Variable, Comparison and Check Stars

Targets	Name	$\alpha_{2000}$	$\beta_{2000}$	$B_{\text{mag}}^{\text{a}}$	$V_{\text{mag}}^{\text{a}}$	$J_{\text{mag}}^{\text{b}}$	$H_{\text{mag}}^{\text{b}}$	$K_{\text{mag}}^{\text{b}}$
Variable star	ATO J108.6991+27.8306	07 14 47.80	+27 49 50.5	14.764	14.224	13.163	12.916	12.925
The comparison	2MASS 07 151 009+2743415	07 15 10.09	+27 43 41.5	15.145	13.982	11.922	11.297	11.200
The Check	2MASS 07 143 242+2751055	07 14 32.42	+27 51 05.5	14.956	14.434	13.330	13.070	13.022

**Notes.**

<sup>a</sup> The *BV*-band magnitudes of the variable, comparison and check stars were determined from the AAVSO Photometric All-Sky Survey DR9 (APASS9; Henden et al. 2016).

<sup>b</sup> The *JHK*-band magnitudes were determined from Two Micron All Sky Survey (2MASS; Cutri et al. 2003).

The observed CCD images were reduced in a standard manner using IRAF.<sup>5</sup> In our work, the differential photometry method was adopted. The basic information about variable, comparison, and check stars are compiled in Table 1. The light curves are shown in Figure 1.

With our observations, the eclipsing times were obtained through the K-W method (Kwee & van Woerden 1956) in Nelson’s program<sup>6</sup> from the *BVRI*-bands light curves. The new eclipsing times and their mean values are shown in Table 2.

### 3. Photometric Analysis

To further understand J108, we analyzed our *BVRI*-band light curves using the 2013 version of the W-D program (Wilson & Devinney 1971; Wilson 1979, 1990, 2008; Wilson et al. 2010; Wilson 2012). We obtained several J108 spectra from LAMOST, as detailed in Table 3, where two spectra provide effective temperatures for the binary of  $6407.81 \pm 96.88$  K and  $6267.75 \pm 24.80$  K. Combined with Gaia DR2 (Gaia Collaboration et al. 2018), DR3 (Gaia Collaboration 2022), and TESS (Paegert et al. 2022) provided effective temperatures of  $6214 \pm 395$  K,  $5888.2 \pm 17.1$  K, and  $6264.9 \pm 18.1$  K, respectively, the average value of  $6208 \pm 110$  K calculated from these temperatures was taken as the effective temperature of the binary. We assumed for the time being that the surface temperature  $T_1$  of the primary component is consistent with this effective temperature. Based on this temperature, the gravity-darkening coefficients and the bolometric albedo were set at  $g_{1,2} = 0.32$  (Lucy 1967) and  $A_{1,2} = 0.5$  (Ruciński 1969) in either binary system, respectively. The bolometric and bandpass limb-darkening were adopted the square-root function laws from the values of van Hamme (1993).

The mass ratio is an important parameter for obtaining a credible photometric solution. Due to the lack of sufficient spectral observations, we used the  $q$ -search method to determine the mass ratio. We searched for the mass ratio of the two components between 0 and 1, i.e., primary component with more massive mass. The results are shown in Figure 2,

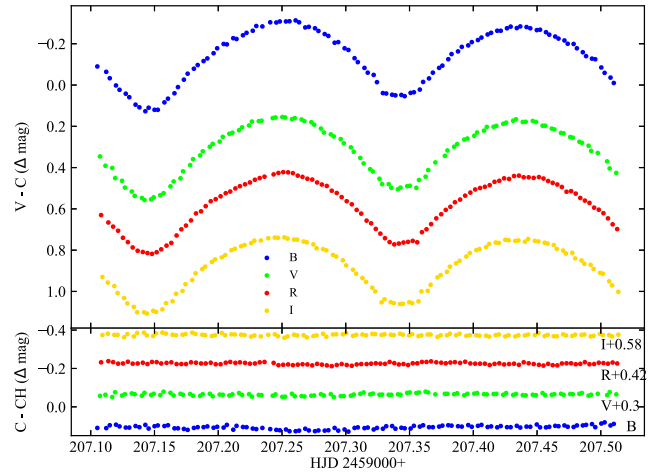


**Figure 1.** Multicolor light curves of J108.

where the initial value of the mass ratio  $q$  entered into the W-D code as an adjustment parameter is 0.168, and this value corresponds to the smallest residual  $\sum \omega_i (O - C)_i^2$ . During the search for the best mass ratio, we found that the massive component has a lower temperature, which means that it is a W-type W UMA binary. Meanwhile, these two components always fill their Roche lobes. We decided to use the W-D program in mode 3 (contact state). In fact, the effective temperature of the binary star differs somewhat from the temperature of its components, and we calculate the surface temperature of each component using the following equation (Christopoulou & Papageorgiou 2013).

$$T_1 = (((1 + k^2)T_{\text{eff}}^4)/(1 + k^2(T_2/T_1)^4))^{0.25}, \quad (1)$$

$$T_2 = T_1(T_2/T_1). \quad (2)$$

The  $k$  in the equation is the radius ratio ( $r_2/r_1$ ),  $T_{\text{eff}}$  is the effective temperature of the binary, and  $T_2/T_1$  is the temperature ratio of the two components in combination with the preliminary fitting results of the W-D program. After several iterations, the main component temperature tends to a definite value. During the solution process, the orbital inclination  $i$ , the average temperature of the secondary

<sup>5</sup> The Image Reduction and Analysis Facility <http://iraf.noao.edu/>.

<sup>6</sup> <https://www.variablestarssouth.org/software-by-bob-nelson/>

**Table 2**  
Newly Obtained Minima Times of J108 in the *BVRI* Bands

HJD( <i>B</i> ) 2459000+	HJD( <i>V</i> ) 2459000+	HJD( <i>R</i> ) 2459000+	HJD( <i>I</i> ) 2459000+	HJD(average) 2459000+	Min.
207.145 45 ± 0.00036	207.144 88 ± 0.00043	207.145 86 ± 0.00022	207.144 52 ± 0.00053	207.145 18 ± 0.00039	primary
207.342 42 ± 0.00052	207.342 42 ± 0.00044	207.342 96 ± 0.00035	207.342 41 ± 0.00019	207.342 55 ± 0.00035	secondary

**Table 3**  
LAMOST Spectral Information of J108

UT Date (yyyy-mm-dd)	HJD (d)	Phase	Subclass	<i>T</i> <sub>eff</sub> (K)	log <i>g</i>	[Fe/H]	Radial Velocity (km s <sup>-1</sup> )
2011 Nov 14	2455880.390798	0.250407	F0				
2011 Dec 07	2455903.249277	0.385092	F4	6407.81 ± 96.88	4.236 ± 0.155	-0.250 ± 0.102	70.63 ± 8.42
2014 Dec 18	2457010.244898	0.744818	F5	6267.75 ± 24.80	4.066 ± 0.033	-0.235 ± 0.018	54.21 ± 4.05

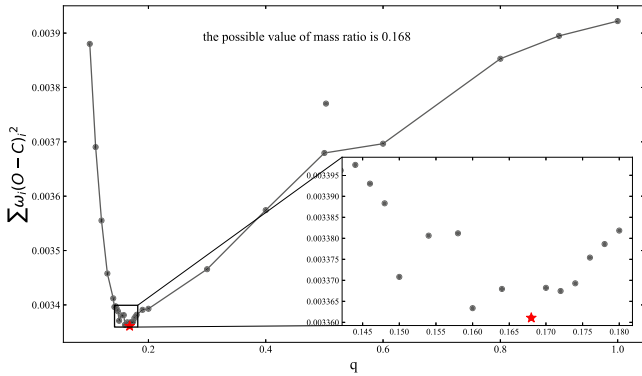


**Figure 2.** Relationships between sum of squares of residuals  $\sum \omega_i(O - C)_i^2$  and the mass ratios  $q$  for J108.

component  $T_2$ , the monochromatic luminosity of the primary component  $L_1$  in the *BVRI* bands, and the dimensionless potential  $\Omega_1 = \Omega_2$  of the two components are adjustable parameters.

We found that the light curves are asymmetric (O’Connell effect, O’Connell 1951) and explain this phenomenon by introducing a starspot model. The photometric solutions are listed in Table 4. The corresponding theoretical light curves that fit the observations better are displayed in Figure 3. From the results in Figure 3, introducing a hot spot in the primary component provides better convergence results, and if another cold spot is added to the secondary component, a better solution with a fill-out factor of  $f = 50.1\%$  and a mass ratio of  $q = 0.1501$  was obtained, as confirmed by the residual values in Table 4. The error in the filling factor of the binary is larger at low mass ratios, because the surface potential through the inner Lagrangian point ( $L_1$ ) and the outer Lagrangian point ( $L_2$ )

are numerically very close. The geometrical structures of J108 at phases of 0.00, 0.25, 0.50, and 0.75 are plotted in Figure 4.

## 4. Discussion and Conclusion

Although J108 had been monitored by many sky surveys, it was neglected for further study. The photometric solutions of this eclipsing binary J108 is presented for the first time. Using the W-D program, we analyzed one set of complete multiple color light curves of the target. Our photometric solutions suggest that J108 is a DLMR binary system with a high degree of overcontact ( $f = 50.1\%$ ) and a derived mass ratio ( $q = 0.1501$ ). The asymmetry of the light curve is explained by a hot spot on the primary and a cold spot on the secondary component. J108 is a W-type W UMa system. According to the photometric results of the three groups of component temperatures, through Table 5 of Pecaut & Mamajek 2013, we could conclude that the spectral type of the primary component is F8, and the spectral type of the secondary component ranges from F5 to F7. The spectral type of these daughter stars differs slightly from the LAMOST results for the spectral type of this binary system in Table 3, which is due to the different spectral type and temperature correspondence criteria.

### 4.1. Absolute Parameters

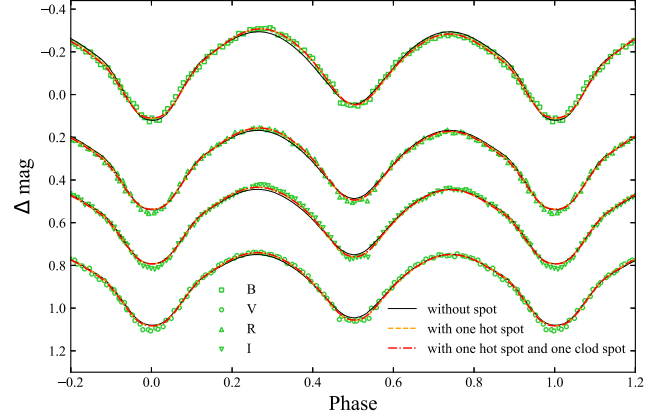
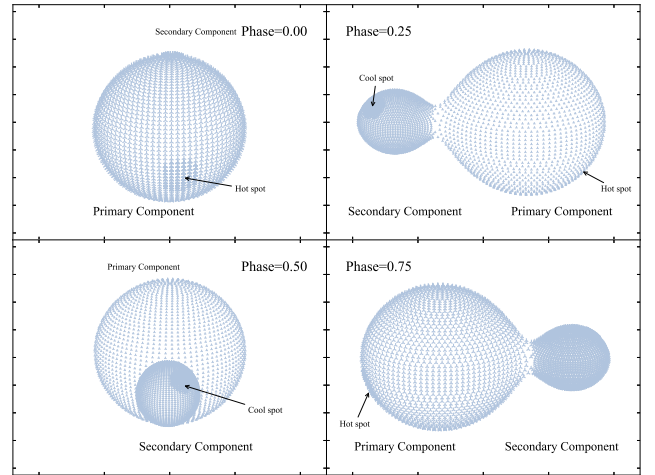
Accurate absolute parameters are obtained for binary star systems with radial velocity curve. In the absence of RV curve, we could use an estimation method to obtain the absolute parameters of the binary system. Since entering the Gaia era, we are able to obtain more accurate distance information. Based on the distance and photometric observations, we are able to obtain the absolute bolometric magnitudes of the components after extinction and reddening corrections. We adopted a similar approach, assuming that the massive component of W UMa is the main sequence star (Yakut & Eggleton 2005). First, the luminosity of the primary star is determined by these equations: (a)

**Table 4**  
 Photometric Elements of J108

Parameters	Without Spots	With One Spot	With Two Spots
$g_1 = g_2$	0.32	0.32	0.32
$A_1 = A_2$	0.5	0.5	0.5
$\Omega_{\text{in}}$	2.07094	2.103 36	2.10336
$\Omega_{\text{out}}$	1.98144	2.006 48	2.00648
$q(M_2/M_1)$	0.1383 ( $\pm 0.0026$ )	0.1501 ( $\pm 0.0016$ )	0.1501 ( $\pm 0.0013$ )
$T_1(\text{K})$	6130 K	6130 K	6130 K
$T_2(\text{K})$	6569 ( $\pm 20$ ) K	6359 ( $\pm 9$ ) K	6254 ( $\pm 10$ ) K
$i^\circ$	71.244 ( $\pm 0.603$ )	72.522 ( $\pm 0.345$ )	72.586 ( $\pm 0.345$ )
$\Omega_1 = \Omega_2$	2.02343 (0.00822)	2.05270 (0.00519)	2.05473 (0.00435)
$L_{1B}/L_B$	0.7859 ( $\pm 0.0067$ )	0.8049 ( $\pm 0.0031$ )	0.8202 ( $\pm 0.0029$ )
$L_{1V}/L_V$	0.8028 ( $\pm 0.0057$ )	0.8137 ( $\pm 0.0028$ )	0.8249 ( $\pm 0.0025$ )
$L_{1R}/L_R$	0.8121 ( $\pm 0.0052$ )	0.8185 ( $\pm 0.0026$ )	0.8275 ( $\pm 0.0024$ )
$L_{1I}/L_I$	0.8189 ( $\pm 0.0049$ )	0.8221 ( $\pm 0.0026$ )	0.8294 ( $\pm 0.0023$ )
$r_1(\text{pole})$	0.5269 ( $\pm 0.0017$ )	0.5209 ( $\pm 0.0011$ )	0.5200 ( $\pm 0.0009$ )
$r_1(\text{side})$	0.5864 ( $\pm 0.0026$ )	0.5778 ( $\pm 0.0016$ )	0.5763 ( $\pm 0.0014$ )
$r_1(\text{back})$	0.6103 ( $\pm 0.0027$ )	0.6025 ( $\pm 0.0017$ )	0.6008 ( $\pm 0.0015$ )
$r_2(\text{pole})$	0.2225 ( $\pm 0.0088$ )	0.2300 ( $\pm 0.0049$ )	0.2300 ( $\pm 0.0040$ )
$r_2(\text{side})$	0.2333 ( $\pm 0.0108$ )	0.2415 ( $\pm 0.0061$ )	0.2414 ( $\pm 0.0049$ )
$r_2(\text{back})$	0.2831 ( $\pm 0.0288$ )	0.2937 ( $\pm 0.0164$ )	0.2933 ( $\pm 0.0131$ )
$f$	53.1 % ( $\pm 9.2$ %)	52.3 % ( $\pm 5.4$ %)	50.2 % ( $\pm 4.5$ %)
Spot 1		Primary	Primary
$\theta(\text{radian})$		0.9291 ( $\pm 0.0534$ )	0.9291 ( $\pm 0.0534$ )
$\phi(\text{radian})$		3.7145 ( $\pm 0.0513$ )	3.7145 ( $\pm 0.0513$ )
$r(\text{radian})$		0.3290 ( $\pm 0.0092$ )	0.3290 ( $\pm 0.0092$ )
$T_s(T_d/T_0)$		1.1959 ( $\pm 0.0083$ )	1.1959 ( $\pm 0.0083$ )
Spot 2			Secondary
$\theta(\text{radian})$			1.9256 ( $\pm 0.0992$ )
$\phi(\text{radian})$			3.3127 ( $\pm 0.0518$ )
$r(\text{radian})$			0.2318 ( $\pm 0.0211$ )
$T_s(T_d/T_0)$			0.9058 ( $\pm 0.0185$ )
$\Sigma W(O - C)^2$	0.00324	0.00203	0.00194

$m_{V_i} - m_{V_{\text{max}}} = -2.5 \log(L_i/L)$ , (b)  $M_{V_i} = m_{V_i} - 5 \log D + 5 - A_V$ , (c)  $M_{\text{bol}_i} = M_{V_i} + BC_{V_i}$ , (d)  $M_{\text{bol}_{1,2}} = 4.73 + 2.5 \log(L_{1,2}/L_\odot)$  (Torres 2010). In our work, the interstellar extinction coefficient  $A_{V_{\text{S\&F}}} = 0.1701 \pm 0.0022$  (mag) (Schlafly & Finkbeiner 2011) from IRSA database<sup>7</sup>, the bolometric corrections  $BC_V = -0.042$  (mag) from Pecaut & Mamajek (2013), distances obtained by Gaia Collaboration (2022), and the maximum visual magnitude  $m_{V_{\text{max}}}$  obtained by fitting ASAS-SN data. Christopoulos et al. (2022) provided a mass–luminosity relationship  $\log L = \log b + a \log M$  ( $b = 0.63 \pm 0.04$  and  $a = 4.8 \pm 0.2$ ). The equations  $M_1 + M_2 = 0.0134a^3/P^2$  and  $R_i = ar_i$  were used. The

<sup>7</sup> <https://irsa.ipac.caltech.edu/applications/DUST/>


**Figure 3.** The photometric precisions of J108 in *BVRI* band.

**Figure 4.** Geometrical structure of J108 with one hot spot on the primary and one cool spot on the secondary at phases of 0.00, 0.25, 0.50, and 0.75.

calculated results are shown in Table 5. Through the mass–luminosity relationship,  $M_1 = 1.331(1) M_\odot$  and  $M_2 = 0.200(2) M_\odot$  were obtained.

## 4.2. Evolutionary States

Based on the absolute parameters, the primary component is plotted in a temperature–luminosity diagram, which is shown in Figure 5. Combined with the [Fe/H] information provided by the LAMOST spectra in Table 3, corresponding to a  $Z$  of about  $0.008 \pm 0.002$ , the tracks of stellar evolution taken from Girardi et al. (2000) with metal abundance  $Z = 0.008$  were chosen. The primary is located between the zero-age main sequence (ZAMS) and the terminal-age main sequence (TAMS) lines, which suggests that the primary component is an evolved MS star. Based on the evolutionary tracks of the

**Table 5**  
Absolute Parameters of J108

Parameters	Value	Error
$D(\text{pc})$	1179.078	25.544
$m_{V\text{max}}(\text{mag})$	14.104	0.025
$m_{V_1}(\text{mag})$	14.313	0.028
$M_{V_1}(\text{mag})$	3.785	0.078
$M_{\text{bol}}(\text{mag})$	3.743	0.078
$L_1(L_\odot)$	2.482	0.177
$L_2(L_\odot)$	0.527	0.047
$M_1(M_\odot)$	1.331	0.001
$M_2(M_\odot)$	0.200	0.002
$a(R_\odot)$	4.800	0.200
$R_1(M_\odot)$	1.470	0.004
$R_2(M_\odot)$	0.660	0.019

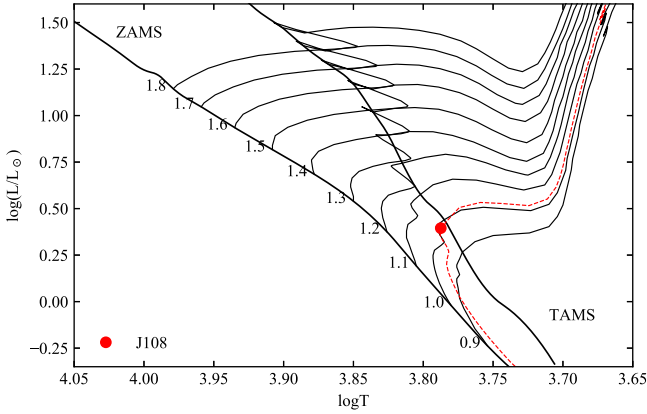


**Figure 5.** Primary component for J108 in the H-R diagram. the zero-age main sequence (ZAMS), the terminal-age main sequence (TAMS), and the evolutionary tracks of each initial mass (from  $0.9 M_\odot$  to  $1.8 M_\odot$ ) and isochrones around the primary component are taken from Girardi et al. 2000 with metal abundance  $Z = 0.008$ . The red dotted line is the isochrone line.

single stars, we estimated the possible evolutionary age of J108 to be  $\sim 7.94$  Gyr.

The mass–radius (M-R) and mass–luminosity (M-L) relations were used to understand the evolutionary state of our target binary. J108 with from Table 7 of Li et al. (2021) for 94 A-type and 85 W-type binaries are plotted in Figure 6. In the figure, the target, like most binary systems, has the higher mass component as the evolved main-sequence star, while the lower mass component of the target has left the main-sequence phase. This could be a mass transfer leading to a mass ratio reversal (Guinan & Bradstreet 1988), meaning that the current low-mass component is the initial high-mass component of the binary system, and this component underwent a rapid mass transfer process as it left the main-sequence phase.

Determining the initial masses of the two components is useful to study the evolution of contact binaries. Since binaries are influenced by their companions during their evolution, the

method of luminosity excess (Yildiz & Doğan 2013) was used to calculate the initial mass of the initial massive component (currently the lower mass component) before the mass transfer process occurred. The initial mass of the secondary  $M_{2i} = 1.83 \pm 0.04 M_\odot$  was obtained using the following equation:

$$M_{2i} = M_2 + 2.50(\delta M - 0.07)^{0.64},$$

$$\Delta M_{2i} = \Delta M_2 + \frac{1.59}{(\delta M - 0.07)^{0.36}} \left( \frac{0.22 \Delta L_2}{L_2^{0.76}} + \Delta M_2 \right), \quad (3)$$

where  $\delta M = M_L - M_2$ ,  $M_2$  is the current mass of the secondary component,  $M_L = (L_2/1.49)^{1/4.216}$ ,  $\Delta$  denote the errors of the corresponding quantity. Based on the possible initial mass ratios, the initial mass range of the primary star was determined ( $M_{1i}$  from  $0.67$  to  $1.21 M_\odot$ ). The initial mass of  $0.985 M_\odot$  obtained from Figure 5 is in this initial mass range, assuming that the primary star is a main sequence single star. The thermal timescale of the more massive star is shorter. When the mass difference between the two components of a binary system is relatively large (about 2.5 times), the evolution of the massive component is faster (Sen et al. 2022). The outer layers of the more massive component expand and break through its Roche radius. The less massive component is subject to unstable dynamical mass transfer and gains mass. The previous timescale required for the thermal adjustment of the smaller mass component is longer than the timescale required for the mass loss of the larger mass component, so the less massive star will expand. When both components expand beyond the Roche critical volume, the binary star evolves into a system with a common envelope (Taam & Ricker 2010; Ivanova et al. 2013). It can be seen that the initial massive component lost a large amount of mass (about  $1.6 M_\odot$ ) when it left the main sequence phase, part of which was transferred to the present primary star (about from  $0.1$  to  $0.66 M_\odot$ ), and another more mass was lost from the binary system (about from  $1$  to  $1.5 M_\odot$ ), which will cause a decrease in the orbital angular momentum of the binary system. The process could be called as the Roche lobe overflow (Hurley et al. 2002; Hirai & Mandel 2022), during which the initial less massive component gains a small fraction of the mass lost by the massive component, and more mass is spilled from the outer Lagrangian points in order to form short-period binary systems, a theory corroborated by our observations.

The equation  $\frac{J_{\text{spin}}}{J_{\text{orb}}} = \frac{1+q}{q} [(k_1 r_1)^2 + (k_2 r_2)^2 q]$  was given by Yang & Qian (2015) to calculate the ratio of the spin angular momentum  $J_{\text{spin}}$  to the orbital angular momentum  $J_{\text{orb}}$ , which reflects the stability of the binary evolution. In this work,  $k_i^2$  is set as  $0.06$  (Li & Zhang 2006) and  $\frac{J_{\text{spin}}}{J_{\text{orb}}} = 0.151$  was obtained,  $J_{\text{spin}}/J_{\text{orb}} < 1/3$  indicates that J108 is currently in a stable evolutionary state.

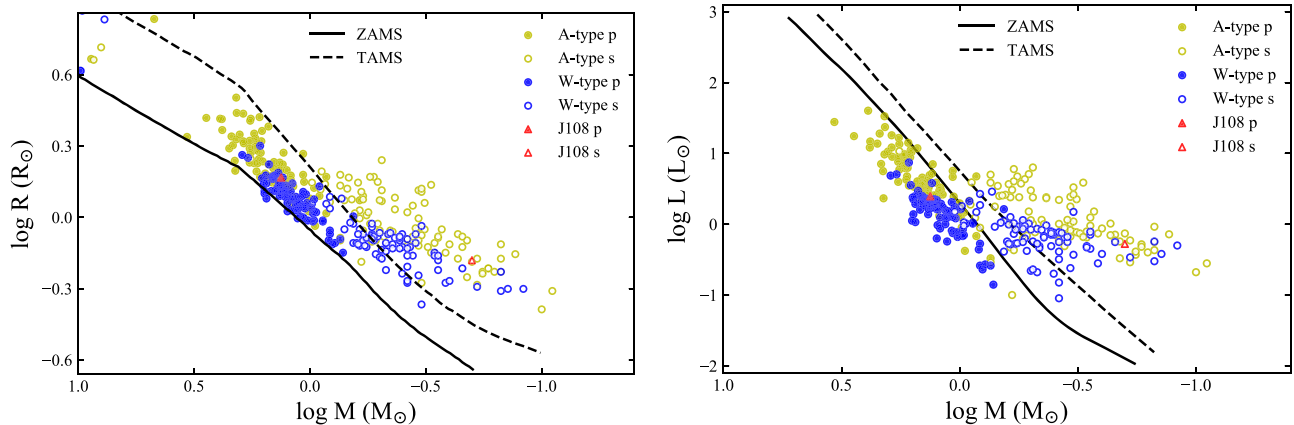


**Figure 6.** The mass–radius diagram (left) and mass–luminosity diagram (right). The solid line and the dashed line, which represent the ZAMS and TAMS respectively, are constructed by the binary system evolution code provided by Hurley et al. (2002). Red regular triangles represent our own two targets. The A-type and the W-type contact binaries from Li et al. (2021) are displayed as yellow circles and blue circles, respectively.

This paper presents the first detailed photometric analysis of ATO J108.6991+27.8306 using multimetric photometric data from NOWT observations. This is a neglected, deep ( $f = 50.1\%$ ), low mass ratio ( $q = 0.1501$ ) W-type W UMA binary system, which implies that it is at a late evolutionary stage of contact binary systems. We have derived the initial masses of the two components and inferred an evolutionary age of the system of about 7.94 Gyr.

The minima of light times that we have collected so far are not enough to support our work on long-term orbital period analysis, so more observations are necessary and the variation of the orbital period needs to be further investigated. The continuous loss of orbital angular momentum is visualized by the decreasing orbital period of the system, which may lead to an increase of the filling factor and a decrease of the inter-binary distance, which will evolve into a rapidly rotating star. Conversely, if the orbital period of the target is continuously increasing, then ATO J108.6991+27.8306 will be more valuable as an idiosyncratic target for research, and more detailed data are needed to support the construction of the theory.

### Acknowledgments

This work is supported by the National Key R&D program of China for Intergovernmental Scientific and Technological Innovation Cooperation Project under No. 2022YFE0126200, the Chinese Academy of Sciences (CAS) “Light of West China” Program, No. 2022-XBQNXZ-013, the Natural Science Foundation of Xinjiang Uygur Autonomous Region, No. 2022D01E86, the National Natural Science Foundation of China under grant U2031204, and the science research grants from the China Manned Space Project with No. CMS-CSST-2021-A08. New CCD photometric observations of the system

were obtained with the 1.0 m telescope (NOWT) at Xinjiang Astronomical Observatory.

### ORCID iDs

Shuo Ma  <https://orcid.org/0000-0002-8324-0506>

### References

- Bai, C.-H., Feng, G.-J., Zhang, X., et al. 2020, *RAA*, **20**, 211  
 Belloni, D., Schreiber, M. R., Pala, A. F., et al. 2020, *MNRAS*, **491**, 5717  
 Binnendijk, L. 1970, *VA*, **12**, 217  
 Bopp, B. W., & Stencel, R. E. 1981, *ApJL*, **247**, L131  
 Borkovits, T., Elkhateeb, M. M., Csizmadia, S., et al. 2005, *A&A*, **441**, 1087  
 Chen, X., Wang, S., Deng, L., et al. 2020, *ApJS*, **249**, 18  
 Christopoulou, P.-E., Lalounta, E., Papageorgiou, A., et al. 2022, *MNRAS*, **512**, 1244  
 Christopoulou, P. E., & Papageorgiou, A. 2013, *AJ*, **146**, 157  
 Cutri, R. M., Skrutskie, M. F., van Dyk, S., et al. 2003, *yCat*, II/246  
 Gaia Collaboration 2022, *yCat*, I/355  
 Gaia Collaboration, Brown, A. G. A., Vallenari, A., et al. 2018, *A&A*, **616**, A1  
 Girardi, L., Bressan, A., Bertelli, G., & Chiosi, C. 2000, *A&AS*, **141**, 371  
 Guinan, E. F., & Bradstreet, D. H. 1988, in *Formation and Evolution of Low Mass Stars*, ed. A. K. Dupree & M. T. V. T. Lago, 241 (Vienna do Castelo: NATO Advanced Study Institute), 345  
 Heinze, A. N., Tonry, J. L., Denneau, L., et al. 2018, *AJ*, **156**, 241  
 Henden, A. A., Templeton, M., Terrell, D., et al. 2016, *yCat*, II/336  
 Hirai, R., & Mandel, I. 2022, *ApJL*, **937**, L42  
 Hoffman, D. I., Harrison, T. E., McNamara, B. J., et al. 2006, *AJ*, **132**, 2260  
 Hurley, J. R., Tout, C. A., & Pols, O. R. 2002, *MNRAS*, **329**, 897  
 Ivanova, N., Justham, S., Chen, X., et al. 2013, *A&ARv*, **21**, 59  
 Jayasinghe, T., Stanek, K. Z., Kochanek, C. S., et al. 2019, *MNRAS*, **486**, 1907  
 Jiang, D. 2020, *MNRAS*, **492**, 2731  
 Khaliullina, A. I. 2018, *Astron. Rep.*, **62**, 520  
 Kwee, K. K., & van Woerden, H. 1956, *BAN*, **12**, 327  
 Lanza, A. F., Rodono, M., & Rosner, R. 1998, *MNRAS*, **296**, 893  
 Li, K., Xia, Q.-Q., Kim, C.-H., et al. 2021, *AJ*, **162**, 13  
 Li, L., & Zhang, F. 2006, *MNRAS*, **369**, 2001  
 Lucy, L. B. 1967, *ZAp*, **65**, 89  
 Lucy, L. B. 1968, *ApJ*, **151**, 1123  
 Ma, S., Liu, J. Z., Zhang, Y., Hu, Q. S., & Lv, G. L. 2022, *RAA*, **22**, 095017  
 Meng, G., Zhang, L.-y., Han, X. L., et al. 2021, *MNRAS*, **503**, 324  
 O’Connell, D. J. K. 1951, *PRCO*, **2**, 85  
 Paegert, M., Stassun, K. G., Collins, K. A., et al. 2022, *yCat*, IV/39

- Panchal, A., & Joshi, Y. C. 2021, *AJ*, 161, 221
- Pecaut, M. J., & Mamajek, E. E. 2013, *ApJS*, 208, 9
- Perets, H. B., & Fabrycky, D. C. 2009, *ApJ*, 697, 1048
- Poru, A., Alicavus, F., Fernández-Lajús, E., et al. 2021, *RAA*, 21, 203
- Qian, S., Yang, Y., Zhu, L., He, J., & Yuan, J. 2006, *Ap&SS*, 304, 25
- Ruciński, S. M. 1969, *AcA*, 19, 245
- Schlafly, E. F., & Finkbeiner, D. P. 2011, *ApJ*, 737, 103
- Sen, K., Langer, N., Marchant, P., et al. 2022, *A&A*, 659, A98
- Shi, X.-D., Qian, S.-B., Li, L.-J., Na, W.-W., & Zhou, X. 2020, *RAA*, 20, 096
- Sikora, J., Rowe, J., Howell, S. B., Mason, E., & Wade, G. A. 2020, *MNRAS*, 496, 295
- Stepien, K. 2006, *AcA*, 56, 199
- Taam, R. E., & Ricker, P. M. 2010, *NewAR*, 54, 65
- Torres, G. 2010, *AJ*, 140, 1158
- van Hamme, W. 1993, *AJ*, 106, 2096
- Wei, D.-D., Wang, B., Chen, H.-L., et al. 2021, *RAA*, 21, 223
- Wilson, R. E. 1979, *ApJ*, 234, 1054
- Wilson, R. E. 1990, *ApJ*, 356, 613
- Wilson, R. E. 2008, *ApJ*, 672, 575
- Wilson, R. E. 2012, *AJ*, 144, 73
- Wilson, R. E., & Devinney, E. J. 1971, *ApJ*, 166, 605
- Wilson, R. E., Van Hamme, W., & Terrell, D. 2010, *ApJ*, 723, 1469
- Yakut, K., & Eggleton, P. P. 2005, *ApJ*, 629, 1055
- Yang, F., Long, R. J., Shan, S.-S., et al. 2020, *ApJS*, 249, 31
- Yang, Y.-G., & Qian, S.-B. 2015, *AJ*, 150, 69
- Yildiz, M., & Doğan, T. 2013, *MNRAS*, 430, 2029